

## ACCURATE COMPUTATION OF MAGNETIC INDUCTION GENERATED BY HV OVERHEAD POWER LINES

Djekidel Rabah<sup>1</sup>, Bessedik Sid Ahmed<sup>1</sup>, Samar Akef<sup>2</sup>

<sup>1</sup>Department of Electrical Engineering, Laghouat University, Algeria

<sup>2</sup>Department of Electrical Engineering, Cairo University, Egypt

**Abstract.** *This paper proposes a 3D quasi-static numerical model for the magnetic induction calculation produced by the high voltage overhead power lines by using the Current Simulation Technique (CST) combined with the Particle Swarm Optimization Algorithm (PSO), in order to determine the appropriate position and number of the filamentary current loops for an accurate computation. The exact form of the catenary of the power line conductors is taken into account in this calculation. From the simulation results, the effect of the conductor sag is largely noticed on the magnetic induction distribution, especially at the mid-span length of the power line where the magnetic induction becomes very significant, the maximum magnetic induction strength at 1 m above the ground level recorded at mid-span point is 8.87  $\mu T$ , at the pylon foot, the maximum value is significantly reduced to 3.94  $\mu T$ . According to these values, we note that the limits set by the ICNIRP guidelines for magnetic induction strength are respected for occupational and public exposure. The simulation results of magnetic induction are compared with those obtained from the 3-D Integration method, a fairly good agreement is found.*

**Key words:** *Current Simulation Technique (CST), Magnetic Induction, Sag Effect, 3-D Integration Method, Particle Swarm Optimization (PSO)*

### 1. INTRODUCTION

The increase in the population leads to raise the energy needed which causes the evolution of the electric energy demand and accelerates the concentration of the transmission lines with a high operating voltage level. These power lines create electric and magnetic fields, and therefore raised serious questions about the potential health and environmental effects associated with high levels of intensity of these fields around these lines. The possible effects of electric and magnetic fields on human health and the environment are discussed in several research projects [1-4]. The limits of exposure to electromagnetic fields (EMF) are derived from the International Commission on Non-

---

Received October 10, 2018; received in revised form February 5, 2019

**Corresponding author:** Djekidel Rabah

Department of Electrical Engineering, University of Amar Telidji of Laghouat, BP 37G route of Ghardaïa, Laghouat 03000, Algeria

(e-mail: [rabah03dz@live.fr](mailto:rabah03dz@live.fr))

Ionizing Radiation Protection (ICNIRP). At Low Frequency 50 Hz, the reference levels for public exposure are 200  $\mu\text{T}$  (magnetic induction) and 5kV/m (electric field). Respectively, the reference levels for occupational exposure are 1 mT and 10kV/m [5].

The accurate evaluation of electric and magnetic fields generated by electric power lines is very important in many areas of research, and necessary in many applications.

In recent years, several publications have been made to calculate the electric and magnetic fields created by power transmission lines. Most assume that the power lines are horizontal straight parallel to a flat ground, and the sag due to the power line weight is neglected or introduced by taking an average height between the maximum and the minimum height of the power line [6-8].

In this paper, in order to obtain a more accurate computational result of the magnetic induction strength distribution around electric power transmission lines, a 3-D quasi-static numerical modeling combining the Current Simulation Technique (CST) with Particle Swarm Optimization (PSO) can be used. The Current Simulation Technique (CST) is an effective approach and more adapted to the simulation of overhead power transmission lines and their particularities such as conductors in bundles and constraints posed by the power lines geometry. It should be noted that this calculation takes into account the effects of the catenary form of the overhead power line conductors.

The major problem in this technique is the optimal number and position coordinates of the filamentary line currents in the sub-conductors [9]. To solve the constraint optimization, we appeal to the Particle Swarm Optimization (PSO) method. PSO is a powerful optimization algorithm that is inspired from the behavior of a flock of birds which is capable of finding global optimum solution [10,11].

In order to verify the accuracy of the combined method, the obtained results are compared with those obtained using 3-D integration approach.

## 2. CURRENT SIMULATION TECHNIQUE (CST)

By analogy with the Charge Simulation Method (CSM) applied to transmission lines to calculate the electric field, it is possible to have a Current Simulation Technique (CST) for calculating the magnetic field on the conductor's lines. In this technique, for a three phase bundled conductor line with  $m$  sub-conductors per phase, each sub-conductor current is simulated by a finite number  $n$  of filamentary line currents distributed on a fictitious cylindrical surface of radius  $R_j$ . The simulation currents  $I_j$ , must satisfy the following conditions [9,12,13]:

1. Zero normal component of the magnetic field strength on the sub-conductors' surfaces, following Biot-Savart law.
2. The sum of the filamentary line currents simulating the sub-conductor current must be equal to the sub-conductor current.

To determine the unknown filamentary currents, a set of equations is formulated at a number of boundary points chosen on the sub-conductors' surface to satisfy the boundary conditions as follows [9,12,13]:

$$A_{ij} = \sum_{j=1}^{3.n.m} P_{ij} \cdot I_j = 0 \quad i = 1, 2, \dots, 3.m.(n-1) \quad (1)$$

$$\sum_{j=(q-1).n+1}^{nq} I_j = I_{cq} \quad q = 1, 2, 3, \dots, 3.m \quad (2)$$

Where,  $P_{ij}$  is the magnetic normal field coefficient determined by the coordinates of the  $i^{\text{th}}$  boundary point and the  $j^{\text{th}}$  filamentary line current and is given by [12]:

$$P_{ij} = \frac{\mu_0}{2\pi} \cdot \ln \frac{R_j}{R_{ij}} \quad (3)$$

Where,  $R_{ij}$  is the distance between simulation current point ( $j$ ) and match point ( $i$ );  $R_j$  is the radius of filamentary line current, as shown in Fig. 1.

We find another expression [9, 13] which uses Equation (4) to calculate the magnetic coefficient.

$$P_{ij} = \frac{1}{2.\pi R_{ij}} \cdot \sin(\theta_{ij}) \quad (4)$$

With,  $\theta_{ij} = \alpha_{ij} - \phi_j$  (see Fig. 1).

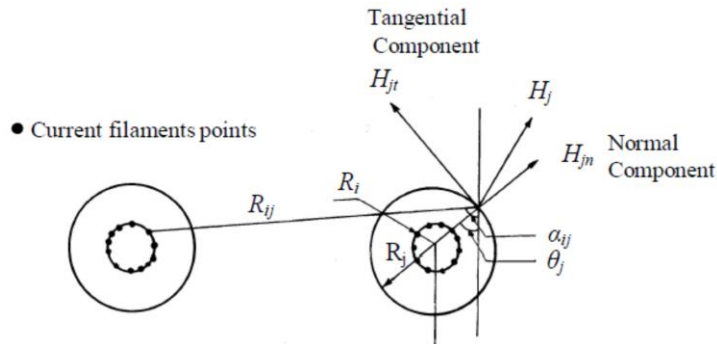


**Fig. 1** Normal and tangential field components at a point on the sub-conductor surface

Once the set of Equations (1) and (2) are solved for the unknown filamentary line currents, the deviation of the normal component of the magnetic field strength from the zero value is calculated at a set of check points (match points) chosen on the sub-conductor's surfaces, the values and positions of simulation currents are known, the distribution of the magnetic field in any region can be calculated easily. The horizontal and vertical components of the magnetic flux density at any point in the space around the HV power line can be calculated by the following equations [12-15]:

$$B_{xj} = -\frac{\mu_0}{2\pi} \cdot \sum_{j=1}^{3.n.m} I_j \cdot \left[ \frac{y_i - y_j}{r_{ij}^2} - \frac{y_i + y_j + D_{erc}}{r_{ij}'^2} \right]$$

$$B_{yj} = \frac{\mu_0}{2\pi} \cdot \sum_{j=1}^{3.n.m} I_j \cdot \left[ \frac{x_i - x_j}{r_{ij}^2} - \frac{x_i - x_j}{r_{ij}'^2} \right]$$
(5)

Where,  $(x_i, y_i)$  and  $(x_j, y_j)$  are the coordinates of the observation point and location of simulation line current, respectively;  $r_{ij}$  is the distance between each conductor and observation point above ground;  $r_{ij}'$  is the distance between each image conductor and observation point (see Fig. 2).

For magnetic field calculation, the image of a filamentary current for a sub-conductor is located at depth different from the real sub-conductor height above ground, is called the depth of penetration; it can be expressed as follows [14]:

$$D_{erc} = 658.87 \cdot \sqrt{\frac{\rho_s}{f}}$$
(6)

Where,  $\rho_s$  is the electrical resistivity of the earth expressed as  $\Omega.m$ ;  $f$  is the frequency of the source current in Hz.

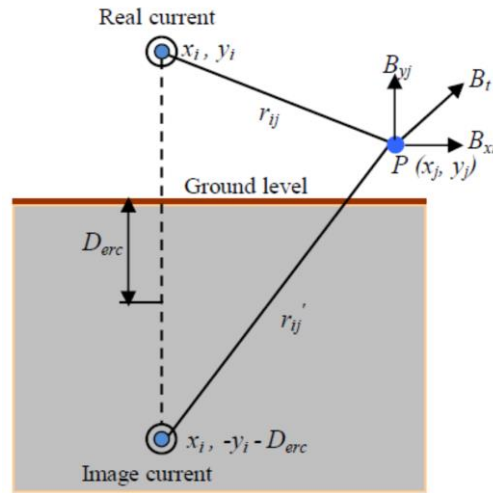


**Fig. 2** Magnetic field generated by a real current and its image in an observation point

The magnitude of the total magnetic induction at any desired point  $P$  is calculated by the summation of the horizontal and vertical components.

$$B_t = \sqrt{B_{xj}^2 + B_{yj}^2}$$
(7)

### 3. PARTICLE SWARM OPTIMIZATION (PSO)

PSO is a robust stochastic optimization algorithm developed by Russell C. Eberhart and James Kennedy in 1995, inspired by the social behavior of bird flocking and fish schooling, it uses a number of agents (particles) that constitute a swarm moving around in the search space for finding global optimal solutions in nonlinear and high-dimensional spaces. In the main loop of the algorithm, the velocities and positions of the particles are iteratively updated by making use of the following equations [16-18]:

$$v_{i+1} = w \cdot v_i + c_1 \cdot R_1 \cdot (P_{best_i} - x_i) + c_2 \cdot R_2 \cdot (G_{best_i} - x_i) \quad (8)$$

$$x_{i+1} = x_i + v_{i+1} \quad (9)$$

Where,  $x_i$  and  $v_i$  are the position and velocity of particle  $i$ ; ( $P_{best_i}, G_{best_i}$ ) are the local best position obtained by the particle  $i$  and the Global best position ever found in the entire population respectively;  $w$  is a parameter controlling the flying dynamics;  $R_1$  and  $R_2$  are random variables in the range  $[0, 1]$ ;  $c_1$  and  $c_2$  are factors controlling the related weighting of corresponding terms.

The PSO algorithm consist the following steps:

1. Initialize the swarm form the solution space
2. Evaluate the fitness of each particle
3. Update individual and global bests
4. Update velocity and position of each particle
5. Go to step2, and repeat until a termination condition has been reached

The objective function (fitness function) used in this method is based on the calculation of the relative error between the magnetic coefficient estimated by the match current points and the magnetic potential of the simulation current points; it is given by the equation below.

$$OF = \frac{1}{n_t} \cdot \sum_{i=1}^{n_t} \left| \frac{A_{c_i} - A_{m_i}}{A_{c_i}} \right| \cdot 100 \quad (10)$$

Where,  $A_{c_i}$  is the magnetic potential calculated by the current points;  $A_{m_i}$  is the new magnetic potential estimated by the match simulation current points;  $n_t$  is the total number of check points.

### 4. 3D INTEGRATION TECHNIQUE

Fig. 3 shows a span of conductor suspended freely between two adjacent pylons, which are at the same level and separated by a horizontal distance  $L$ , takes the form of a catenary curve providing the conductor is perfectly flexible and conductor weight is uniformly distributed along its length [19-25].

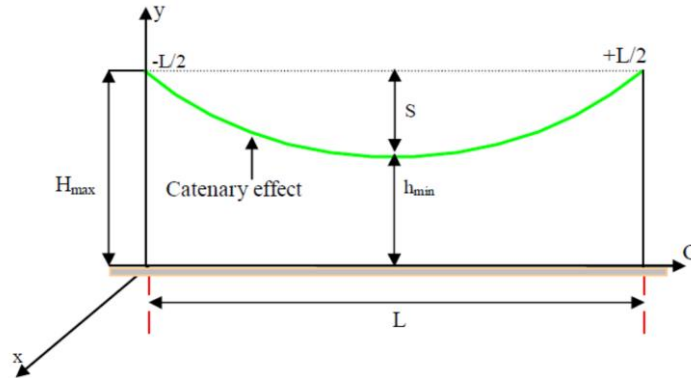


**Fig. 3** The basic catenary geometry for a single conductor line

The equation of the catenary shape of conductor placed in the  $yz$  plane is given by:

$$y(z) = h_{min} + 2.\alpha.\sinh^2\left(\frac{z}{2.\alpha}\right) \quad (11)$$

Where,

$z$  is the longitudinal position of the conductor about  $z$  axis, for a symmetrical line, you normally choose  $z = 0$  at the mid-span;

$h_{min}$  is the minimum height at mid span;

$H_{max}$  is the maximum height on the extremes of the line;

$\alpha$  is the solution of the transcendental equation.

$$2.\frac{H-h}{L}.u = \sinh^2(u) \quad (12)$$

With:  $u = (L/4.\alpha)$

$L$  is the length of the conductor between two pylons, in meters.

The parameter  $\alpha$  is also associated with the mechanical parameters of the line (Catenary constant):

$$\alpha = \frac{T_h}{w_c} \quad (13)$$

Where,  $T_h$  is the horizontal tension at the low point of the conductor curve (N);  $w_c$  is the linear weight of conductor (N/m).

Fig. 4 shows the profile of the catenary of an overhead conductor. The magnetic induction generated by a sagging conductor of an overhead power line with span  $L$  between pylons in an arbitrary point  $P(x_0, y_0, z_0)$  can be determined by applying Biot-Savart law, as [21-25]:

$$\vec{B} = \frac{\mu_0}{4.\pi} \int_l \frac{I.d\vec{l}.\vec{r}}{|r|^3} \quad (14)$$

Where,

$\mu_0$  is the permittivity of free space;  $I$  is the line current;  $\vec{r}$  is the distance vector from the source point  $(x,y,z)$  to the field point  $P(x_0,y_0,z_0)$ , it is given by:

$$\vec{r} = (x - x_0)\vec{i} + (y - y_0)\vec{j} + (z - z_0)\vec{k} \tag{15}$$

$d\vec{l}$  is the differential element at the direction of the current, from the geometry shown in Fig. 4 it results,

$$d\vec{l} = dy_0\vec{j} + dz_0\vec{k} = \sinh\left(\frac{z_i}{\alpha}\right) dz_0\vec{j} + dz_0\vec{k} \tag{16}$$

The magnetic field produced by a multi-phase sagging conductors ( $M$ ), and their images by taking the effect of a conducting ground into account, in any point above the ground placed at span length would be determined applying the superposition principle. The expression for the total magnetic field is given by [14, 21-25]:

$$\vec{B}_{res} = \sum_{i=1}^M [(\vec{B}_{xi})\vec{a}_x + (\vec{B}_{yi})\vec{a}_y + (\vec{B}_{zi})\vec{a}_z] \tag{17}$$

Where:

$$B_{xi} = \frac{\mu_0 I_i}{4\pi} \int_{-L/2}^{L/2} \left[ \frac{\sinh(z_i/\alpha).(z - z_i) - (y - y_i)}{d_i} - \frac{\sinh(z_i/\alpha).(z - z_i) - (y + y_i + D_{erc})}{d'_i} \right] dz_i \tag{18}$$

$$B_{yi} = \frac{\mu_0 I_i}{4\pi} \int_{-L/2}^{L/2} \left[ \frac{(x - x_i)}{d_i} - \frac{(x - x_i)}{d'_i} \right] dz_i \tag{19}$$

$$B_{zi} = \frac{\mu_0 I_i}{4\pi} \int_{-L/2}^{L/2} \left[ \frac{-\sinh(z_i/\alpha).(x - x_i)}{d_i} + \frac{\sinh(z_i/\alpha).(x - x_i)}{d'_i} \right] dz_i \tag{20}$$

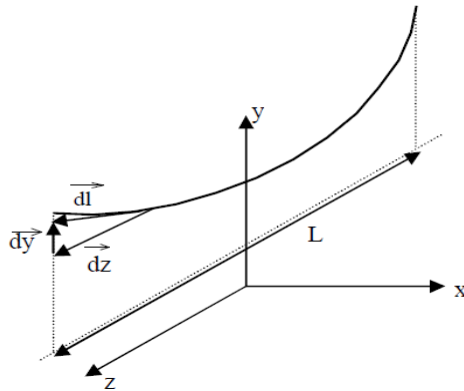


**Fig. 4** Sagging conductor of an overhead power line between two adjacent pylons

With:

$$d_i = [(x - x_i)^2 + (y - y_i)^2 + (z - z_i)^2]^{3/2} \quad (21)$$

$$d'_i = [(x - x_i)^2 + (y + y_i + D_{erc})^2 + (z - z_i)^2]^{3/2} \quad (22)$$

Where,  $(x_i, y_i, z_i)$  being the coordinates of the conductor and  $L$  the distance between two towers (the span length).

It should be recalled that this calculation takes into account the induced currents circulating in the earth wires. These currents can be calculated by the relation given below [18].

$$[I_g] = -[Z_{ii}^{-1}] \cdot [Z_{ij}] \cdot [I_c] \quad (23)$$

Where,

$Z_{ii}$  is the self impedances matrix of the earth wires;

$Z_{ij}$  is the mutual impedances between the phase conductors and earth wires;

$I_c$  is the matrix of currents passing through the phase conductors.

The self and mutual impedances per unit length by means of Carson-Clem formulae are given by [18-26]:

$$Z_{ii} = R_i + \pi^2 \cdot f \cdot 10^{-4} + j \cdot \omega \cdot 2 \cdot 10^{-4} \cdot \left[ \ln \left( \frac{D_{erc}}{R_{GM}} \right) \right] \quad \left[ \frac{\Omega}{km} \right] \quad (24)$$

$$Z_{ij} = \pi^2 \cdot f \cdot 10^{-4} + j \cdot \omega \cdot 2 \cdot 10^{-4} \cdot \ln \left( \frac{D_{erc}}{D_{ij}} \right) \quad \left[ \frac{\Omega}{km} \right] \quad (25)$$

Where,  $R_i$  is the DC resistance per unit length of conductor in ( $\Omega/km$ );  $R_{GM}$  is the geometric mean radius of the conductor in (m);  $D_{ij}$  is the distance between the centers of two conductors of the power line;  $\omega$  is the angular frequency and  $D_{erc}$  is the depth of equivalent earth return conductor given in Equation (6).

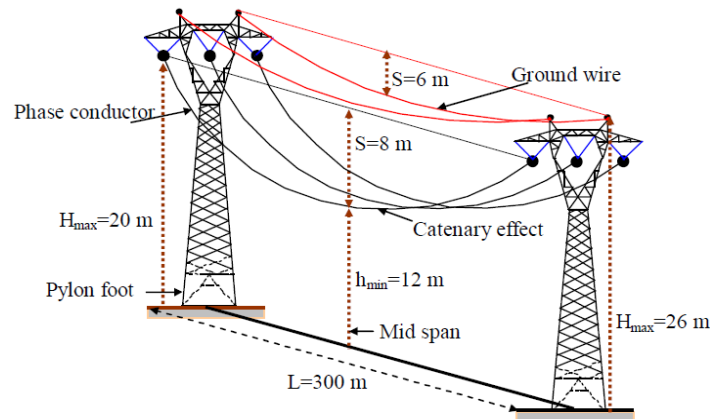


**Fig. 5** Tower-to-tower geometry, showing mid-span between two towers

In the present work, a single-circuit overhead power line of 275 kV, with a symmetrical horizontal phase conductor configuration and two earth wires is considered (see Fig. 5). The three-phase currents on the power line have been assumed under balanced operation with the magnitude of 500A. The Earth is assumed to be homogeneous with a resistivity of 100 Ω.m. Nominal frequency  $f = 50$  Hz.

The simplified schematic diagram of this transmission line structure used in this proposed study, with the arrangement and geometric details in the vicinity of the suspension pylon is shown in Fig.6.

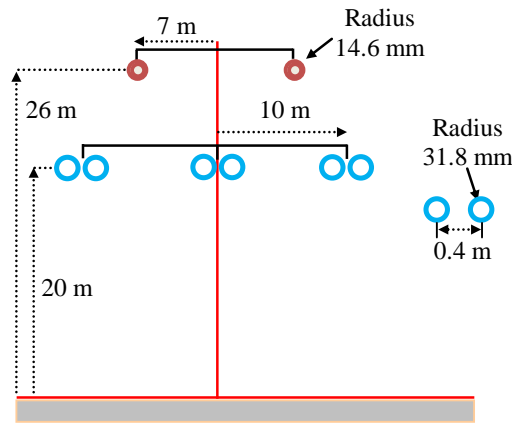


**Fig. 6** 275 kV Single circuit three phase overhead transmission line

### 6. RESULTS AND DISCUSSIONS

The first step in this study is to determine the values of the currents induced in the ground wires of the power line in order to take into account the effect of these currents.

$$I_{g1} = 18.41e^{j^{98}(65.21)^{\circ}} (A), I_{g2} = 18.51e^{j^{98}(-162.98)^{\circ}} (A)$$

The second step consists in determining the optimal values of the number of the current filaments points and their locations; this optimization of the search for the best parameters is made using a particle swarm optimization algorithm (PSO).

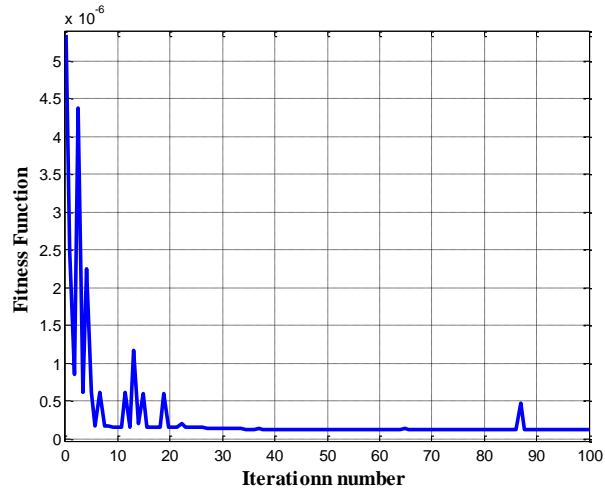
The input parameters used in the PSO algorithm and CST technique are presented in Table 1.

**Table 1** Parameters settings used for the PSO algorithm and CST technique

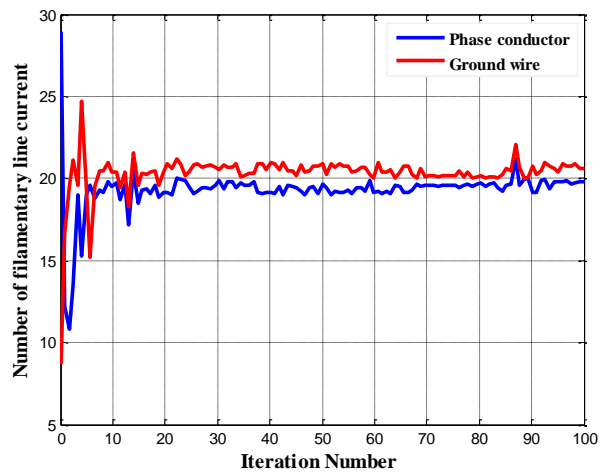
Algorithm+CST	Parameters
Current Simulation Technique (CST)	Range of current filaments points 2–30
	Range of Fictitious radius for conductor phase: 0.01–0.1 [m]
	Range of Fictitious radius for ground wire: 0.003–0.013 [m]
Particle Swarm Optimisation algorithm (PSO)	swarm size $N=20$ , learning factors $c1=c2=2$ , Weights: $W_{min}=0.5$ and $W_{max}=0.5$ , Iteration Max= 100

The convergence of the objective function mentioned above in Equation (10) with the number of iterations is shown in Fig. 7, in order to determine the better solution according to the search space.

The search process of this algorithm at successive iterations with optimal solutions are represented in Figs. 8 and 9 respectively, where it becomes clear that the PSO algorithm converge rapidly to these values.



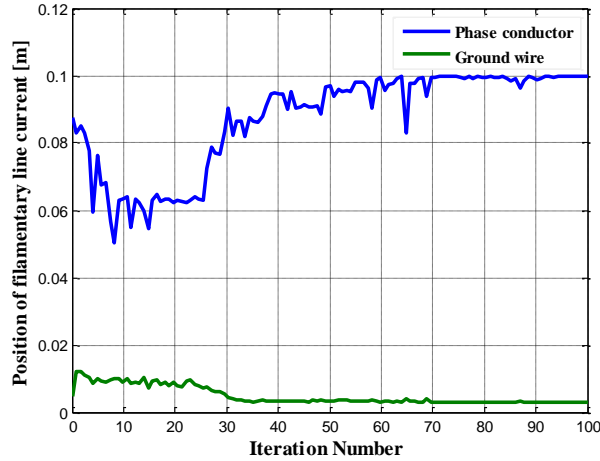
**Fig. 7** Convergence of objective function used in PSO algorithm



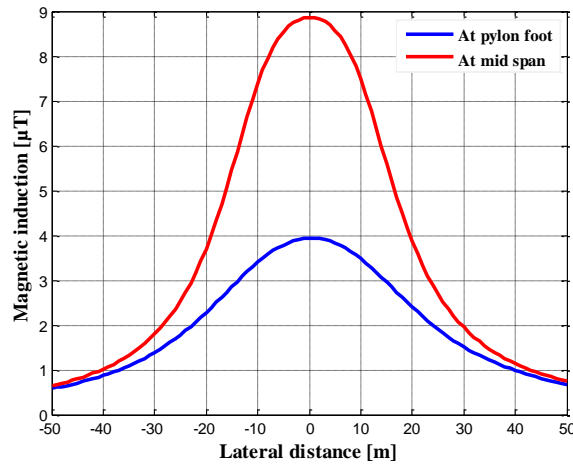
**Fig. 8** Convergence of the optimum values of number of filamentary line current

Fig. 10 shows the magnetic induction distribution under the power line in 1 m from the ground level at pylon foot and mid-span in different points along the transmission line

corridor. It can be seen that magnetic induction is maximum under the middle phase conductor and it decreases rapidly with the lateral distance. Generally, it can be said that the magnetic induction distribution follows a nearly Gaussian shape.



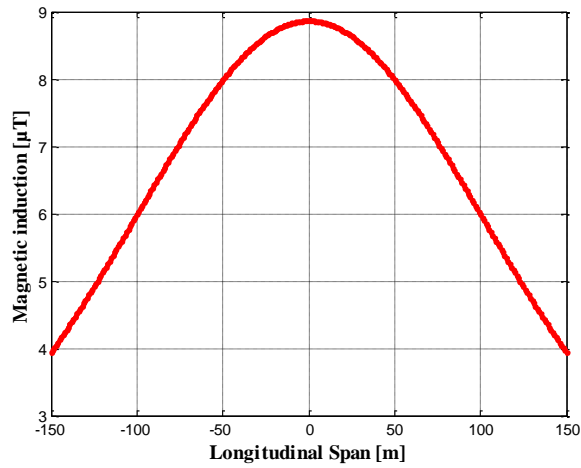
**Fig. 9** Convergence of the optimum values of position of filamentary current



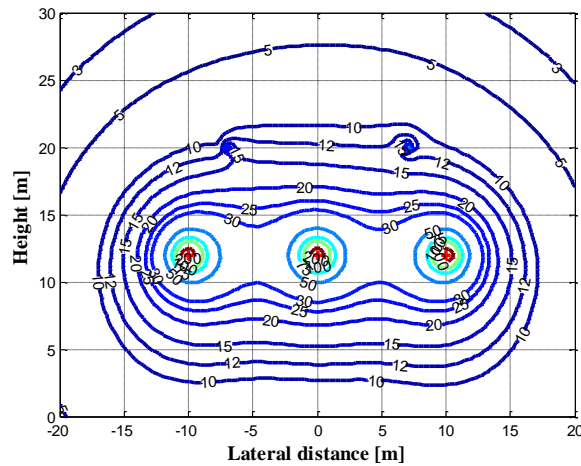
**Fig. 10** Magnetic induction profile at mid-span and pylon foot calculated at 1m above the ground level

Fig. 11 illustrates the longitudinal profile of the magnetic induction under the middle phase conductor, at the point where the magnetic induction is greatest; the magnetic induction strength immediately below the lowest point of a power line (mid-span) is significantly higher than in the proximity of a pylon and at some distance from the line. This illustrates that taking into account the effect of the sag of the conductor in the magnetic induction calculation is a very practical means to model the real behavior of the

power line. Consequently, the maximum value of the magnetic induction increases from  $3.94 \mu\text{T}$  at the pylon foot to  $8.87 \mu\text{T}$  at the half span length, this is due to the sag influence. It is important to mention that the maximum values obtained of the magnetic induction are below the threshold defined by the ICNIRP guidelines.



**Fig. 11** Longitudinal magnetic induction profile calculated at 1m above the ground level



**Fig. 12** Contours lines of the magnetic induction strength around the phase conductors

The contour lines for the magnetic induction distribution around the power line at any point for the  $xy$  plane are depicted in Fig. 12. The magnetic induction magnitudes are highest around and under the power lines and decrease rapidly with the distance from the pylon axes. The different level of magnetic induction is due to the variation of coordinates  $(x, y)$  of the calculation points from the ground level.

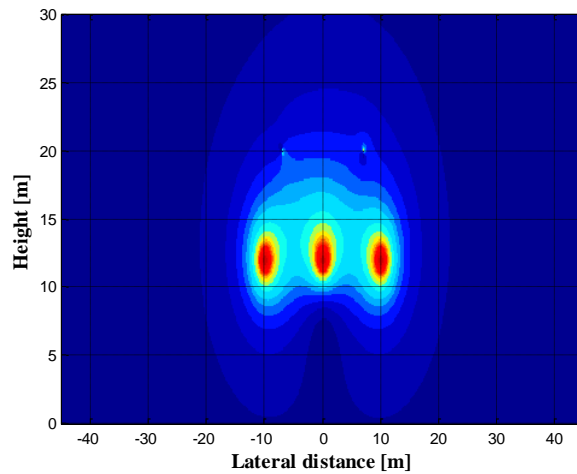


**Fig. 13** Mapping of the magnetic induction generated by the HV power line

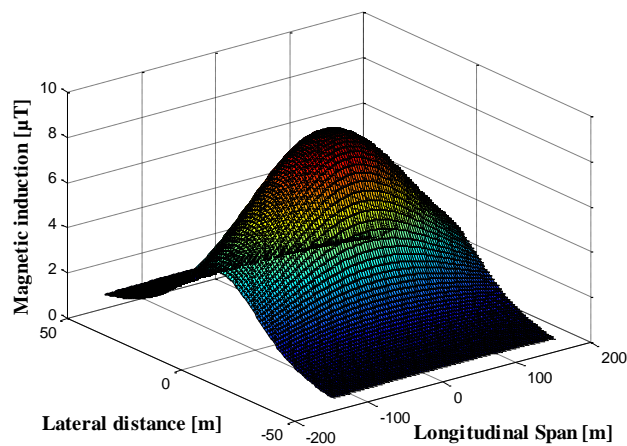
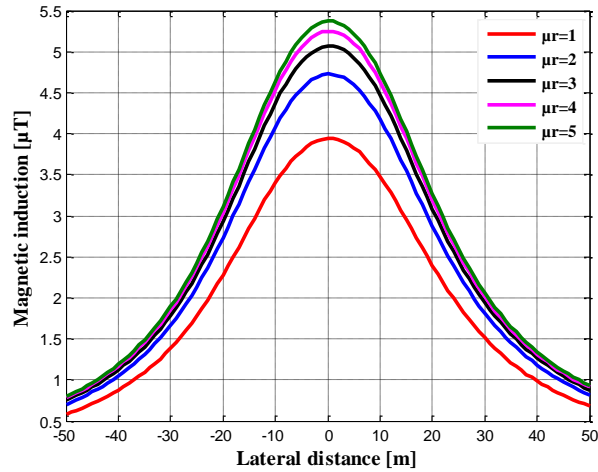


**Fig. 14** Three-dimensional (3-D) magnetic induction profile at 1m above the ground level

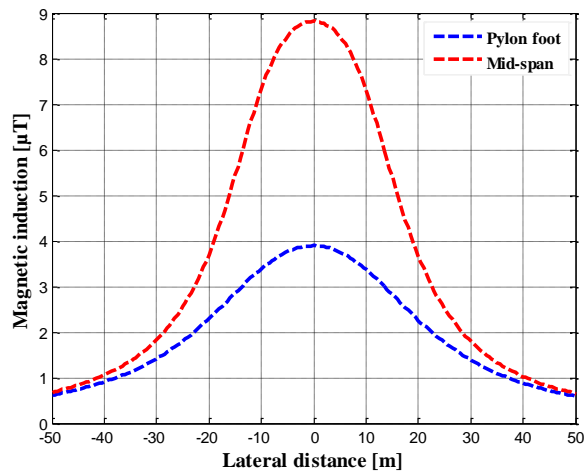
Fig. 13 describes the mapping of the magnetic induction of power line, in an area defined by the vertical coordinates, and the axis of the lateral distance from the pylon axes. It may be interesting to note that the concentrated level of the magnetic induction is produced around the surface of the phase conductors; the magnetic induction gradually decreases with increasing the lateral distance from the center of the power line in both directions of the transmission line corridor.

Fig. 14 shows the three-dimensional profile of the magnetic induction over an area equivalent to a right of way either side of the transmission line center and a longitudinal span between the suspension pylons. It will be noted that the concentrated level of the

magnetic induction exists in a small area under and in the immediate vicinity of the conductors in the mid-span, and then it decreases slowly toward the pylons and even with the increasing of lateral distance from the power line center in both directions along the right-of-way corridor.



**Fig. 15** Magnetic induction profiles for different relative permeability values of soil at pylon foot



**Fig. 16** Magnetic induction profile at mid-span and pylon foot calculated at 1m above the ground level obtained with the analytical formula of magnetostatic

Fig. 15 shows the effect of the soil relative permeability at 1 m above the ground level on the lateral profile of the magnetic induction underneath the power line at pylon foot. An increase in the relative permeability of the soil in the range investigated will result in a slight increase of the magnetic induction.

Fig. 16 shows the magnetic induction profile by modelled the original conductors with the single current filament located in the center of the conductor cross-section, for the same geometrical configuration, the results obtained of the magnetic induction at mid-span and pylon foot are approximately similar to those obtained by the Current Simulation Technique (CST)

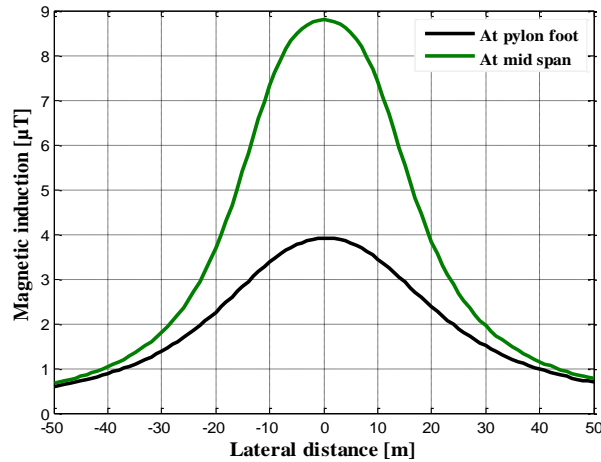
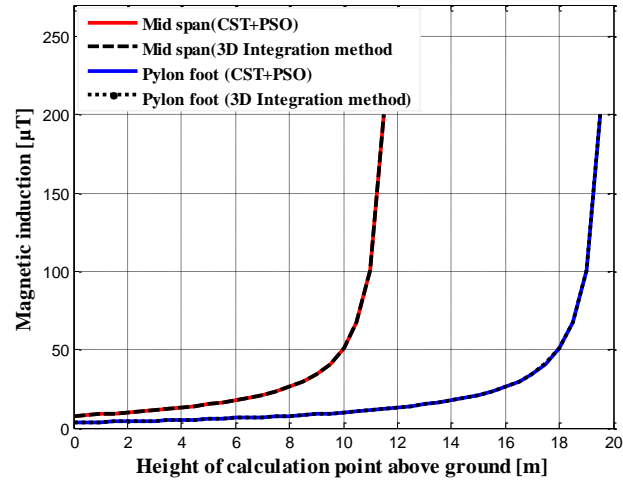


**Fig. 17** Magnetic induction profile in 1 m from the ground level calculated by the 3-D Integration method

In order to validate the adopted method in this study, 3-D Integration method was proposed taking under consideration the conductors sag.

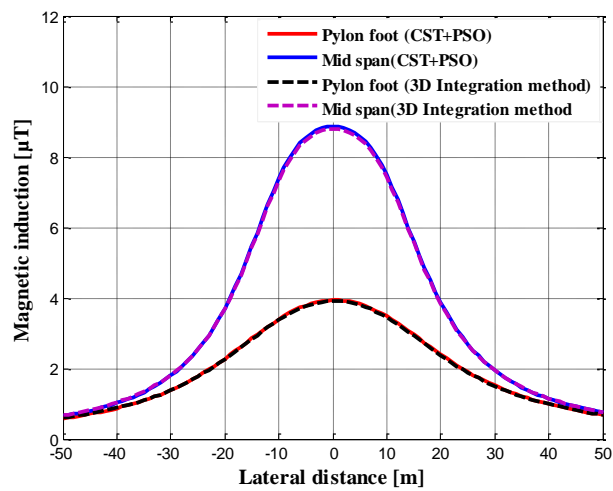
Fig. 17 shows the lateral distribution of the magnetic induction calculated by 3-D Integration method at 1 m above ground level at pylon foot and mid-span length, the magnetic induction is maximum at the center of the power line and then gets progressively reduced as one moves away from the center of the transmission line corridor to achieve very negligible values far from the power line center.

Fig. 18 illustrates the effect of the variation of the calculation point height on the magnetic induction above the ground at the point where the latter is maximum (under the middle phase conductor  $x = 0$ ), using the combined method and 3-D Integration technique. It can be seen that the increase in the calculation point height can lead to an increase in the amplitude of the magnetic induction. Therefore, the magnetic induction values calculated in the vicinity of the surface of phase conductors using the combined method are well correlated with those obtained by the 3-D integration technique. The graphs of two methods are perfectly superposed.



**Fig. 18** Magnetic induction profile as a function of the observation point height above ground

The obtained results of the lateral distribution of magnetic induction computed by the combined method CST+PSO were compared with those calculated by the 3-D Integration method as shown in Fig. 19, a very good agreement is achieved, the two graphs are perfectly superimposed.



**Fig. 19** Comparison of magnetic induction levels between the proposed method and 3-D Integration method

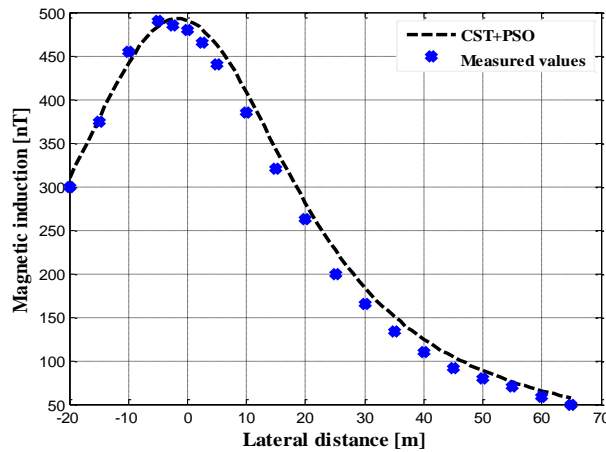


**Fig. 20** Comparison between the magnetic induction values using the proposed method and with those measured described in reference [22]

In order to confirm the accuracy of the presented method, the obtained results were compared with the measured values available in the literature [22]. As can be seen from this comparison shown in Fig. 20, the simulated values of the magnetic induction resemble those measured. Another point to note that the majority of the measured values at 1 m above the ground level are lower than the calculated values because of the metallic objects located in the immediate vicinity of the power line which act as shielding means are neglected, and once again, a very good agreement is achieved which validates the accuracy of the presented method.

## 7. CONCLUSIONS

In this paper, a 3D quasi static numerical modelling for computation of the magnetic induction generated by overhead power lines is presented, in order to obtain the most appropriate position and number of filamentary current loops used in Current Simulation Technique (CST) which provides the solution of sufficient accuracy, a Particle Swarm Optimization algorithm (PSO) is applied. From the results, it is clear that the magnetic induction strength is maximum at the center of the power line, and then decreases with increase in the lateral distance, the magnetic induction strength immediately below the lowest point of the power line is significantly higher than in the proximity of the pylon and at some distance from the line, the magnetic induction around the pylon is much lower than at mid-span. The obtained result showed that the calculated magnetic induction under the HV power line is within the ICNIRP safety limit for general public and occupational exposure. The obtained results by the proposed method were compared with those obtained by the 3-D Integration method. The simulation results are almost identical and are visually superimposed; the comparison is satisfying enough and it sufficient to confirm the accuracy of the combined method.

## REFERENCES

- [1] Ch. J. Portier, M.S. Wolfe, "Assessment of Health Effects from Exposure to Power Line Frequency Electric and Magnetic Fields", Working Group Report, NIEHS and EMFRAPID, August 1998.
- [2] K. Olden, "Health Effects from Exposure to Power-Line Frequency Electric and Magnetic Fields", National Institute of Environmental Health Sciences, NIEHS Report, PL 102-486, Section 2118, 1999.
- [3] M. Havas, "Biological Effects of Low Frequency Electromagnetic Fields", Chapter 10, *Electromagnetic Environments and Health in Buildings*, Spon Press, London, pp. 207-232, 2004.
- [4] T. Samaras, "Preliminary Opinion on Potential Health Effects of Exposure to Electromagnetic Fields", Scientific Committee on Emerging and Newly Identified Health Risks SCENIHR, Health effects of EMF, November 2013.
- [5] ICNIRP, "International Commission on Non-Ionizing Radiation Protection, "Guidelines for limiting exposure to time-varying electric and magnetic fields (1Hz to 100 kHz) ", *Health Physics*, vol. 99, no.6, pp. 818–836, 2010.
- [6] Cigré, "Electric and Magnetic Field Produced by Transmission Systems", Working Group 01 (Interference and Fields) of Study Committee 36, Paris, 1980.
- [7] M.L.P. Filho, J.R. Cardoso, C.A.F. Sartori, M.C. Costa, B.P. de-Alvarenga, A.B. Dietrich, L. M. R. Mendes, "Upgrading Urban High Voltage Transmission Line: Impact on Electric and Magnetic Fields in the Environment", In *Proceedings of the IEEE/PES Transmission and Distribution Conference and Exposition*, vol. 8, 2004, pp. 788–793.
- [8] K. A. Vyas, J. G. Jamnani, "Analysis and Design Optimization of 765 kV Transmission Line Based on Electric and Magnetic Fields for Different Line Configurations", In *Proceedings of the IEEE 6th International Conference on Power Systems (ICPS)*, March 2016, pp. 1–6.
- [9] M. Abdel-Salam, H. Abdallah, M. Th. El-Mohandes, H. El-Kishky, "Calculation of Magnetic Fields From Electric Power Transmission Lines", *Electric Power Systems Research*, vol. 49, no. 2, pp. 99–105, March 1999.
- [10] R. Djekidel, A. Ameer, D. Mahi, A. Hadjadj, "Electrostatic Interference Calculation From H-V Power Lines to Aerial Pipelines Using Hybrid PSO-CSM Approach", In *Proceedings of the IEEE 9th Jordanian International Electrical and Electronics Engineering Conference*, pp.1–6, Oct 2015.
- [11] S. A. Bessedik, H. Hadi, "Prediction of Flashover Voltage of Insulators Using Least Squares Support Vector Machine with Particle Swarm Optimization", *Electric Power Systems Research*, vol. 104, pp. 87–92, 2013.
- [12] D. Yao, B. Li, J. Deng, D. Huang, X. Wu, "Power Frequency Magnetic Field of Heavy Current Transmit Electricity Lines Based on Simulation Current Method", In *Proceedings of the IEEE Automation Congress*, 2008, pp. 1–4.
- [13] R. Radwan, M. Abdel-Salam, A.B. Mahdy, M. Samy, "Laboratory Validation of Calculations of Magnetic Field Mitigation Underneath Transmission Lines Using Passive and Active Shield Wires", *Innovative Systems Design and Engineering*, vol. 2, no. 4, pp. 218–232, 2011.
- [14] J.R. Riba Ruiz, A. G. Espinosa, "Magnetic Field Generated by Sagging Conductors of Overhead Power Lines", *Computer Applications in Engineering Education*, vol. 19, no 4, pp.787–794, 2011.
- [15] A. R. Memari, W. Janischewskij, "Mitigation of Magnetic Field near Power Lines", *IEEE Transactions on Power Delivery*, vol. 11, no. 3, pp. 1577–1586, Jul 1996.
- [16] J. Kennedy, R. C. Eberhart, "Particle Swarm Optimization", In *Proceedings of the IEEE International Conference on Neural Networks*, Australia, vol. 19, 1995, pp. 1942–1948.
- [17] F. Rebahi, A. Bentounsi, H. Bouchekara, R. Rebbah, "Optimization Design of a Doubly Salient 8/6 SRM Based on Three Computational Intelligence Methods", *Turkish Journal of Electrical Engineering & Computer Sciences*, vol. 24, no. 5, pp. 4454–4464, 2016.
- [18] R. Djekidel, S. A. Bessedik, P. Spiteri, D. Mahi, "Passive Mitigation for Magnetic Coupling between HV Power Line and Aerial Pipeline using PSO Algorithms Optimization", *Electric Power Systems Research*, vol. 165, pp. 18–26, 2018.
- [19] K. Budink, W. Machczynski, J. Szymenderski, "Voltage Induced by Currents in Power Line Sagged Conductors in Nearby Circuits of Arbitrary Configuration", *Archives of electrical engineering*, vol. 64, no. 2, pp. 227–236, 2015.
- [20] M. P. Arabani, B. Porkar, S. Porkar, "The Influence of Conductor Sag on Spatial Distribution of Transmission Line Magnetic Field", Cigre, Paris, Paper B2-202, 2004.
- [21] A. Z. El-Dein, "Magnetic-Field Calculation Under EHV Transmission Lines for More Realistic Cases", *IEEE Transactions on Power Delivery*, vol. 24, no. 4, pp. 2214–2222, Oct 2009.

- [22] I. N. Ztoupis, I. F. Gonos, I. A. Stathopoulos, "Calculation of Power Frequency Fields from High Voltage Overhead Lines in Residential Areas", In Proceedings of the 18th International Symposium on High Voltage Engineering, paper A-01, 2013, pp. 61–69.
- [23] K. Deželak, G. Stumberger, F. Jakl, "Emissions of Electromagnetic Fields Caused by Sagged Overhead Power Lines", *Przegląd Elektrotechniczny*, vol. 87, no. 3, pp. 29–32, 2011.
- [24] M. Perić, S. Aleksić, "Influence of Conductor Sag on Magnetic Field Distribution in Vicinity of Power Lines", *International Journal of Emerging Sciences*, vol. 1, no. 4, pp. 564–574, December 2011.
- [25] A. Z. El-Dein, "The Effects of the Span Configurations and Conductor Sag on the Magnetic Field Distribution under Overhead Transmission Lines", *Journal of Physics*, vol. 1 no. 2, pp. 11–23, July 2012.
- [26] M. Albano, R. Turri, S. Dessanti, A. Haddad, H. Griffiths, B. Howat, "Computation of the Electromagnetic Coupling of Parallel Untransposed Power Lines", *IEEE Power Engineering Conference*, vol. 1, pp. 303-307, 2006.